ACS OMEGA

http://pubs.acs.org/journal/acsodf

Article

Aluminum Hydroxide Nano- and Microstructures Fabricated Using Scanning Probe Lithography with KOH Ink

Jehyeok Ryu, Jeong-Sik Jo, Jin-Hyun Choi, Deuk Young Kim, Jiyoun Kim, Dong Hyuk Park,* and Jae-Won Jang*

Cite This: *ACS Omega* 2023, 8, 10439−10448

Read Online

ACCESS | Metrics & More | Article Recommendations | Supporting Information

ABSTRACT: Using scanning probe lithography (SPL) with KOH ink, this study fabricates aluminum hydroxide ($Al(OH)_3$) nano- and microfeatures on a gold (Au) film that has been deposited on an aluminum (Al) layer. Hydroxyl ions (OH^-) from the KOH ink loaded onto the Au film can react with the underlying Al layer to form $Al(OH)_3$ structures due to the decrease in the pH of the reacting solution.[1] In this process, $Al(OH)_3$ solidification is governed by the pH of the KOH ink solution, which is affected by its volume. Suitably small volumes (down to hundreds of attoliters) of the KOH ink solution can be applied to the substrate surface using dip-pen nanolithography (DPN) and polymer-pen lithography (PPL). Using DPN and PPL printing with the solid (i.e., gel) and liquid phases of KOH ink, sub-micron- (minimum ≈300 nm) and micron-sized (≥4 μm) $Al(OH)_3$ features can be obtained, respectively. The fabrication of $Al(OH)_3$ structures using the proposed pH-dependent solidification process can be achieved with relatively small volumes in ambient conditions without requiring a previously reported molding process.[1,2]

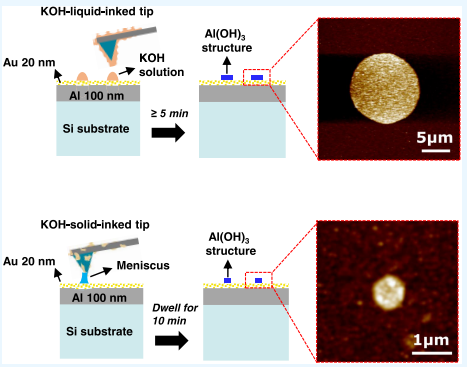

INTRODUCTION

The gold (Au) nanomembrane-based lithography process developed by our group to produce $Al(OH)_3$ nano- and microfeatures utilizes a thin Au film (less than 50 nm thick) as a hydroxyl ion (OH^-) channel due to the porosity of the Au film[1,2] allowed by island growth (Volmer−Weber growth).[3] The OH^- supplied by a KOH solution dropped onto this Au nanomembrane (the thin Au film with porosity) can react with the underlying aluminum (Al) layer. Depending on the pH of the reacting OH^- solution, solid aluminum hydroxide ($Al(OH)_3$) can be produced. In general, Al forms soluble aluminum hydroxide ($Al(OH)_4^-$) when it reacts with OH^-; however, when the pH of the reacting solution is sufficiently low, soluble $Al(OH)_4^-$ is converted to solid $Al(OH)_3$. If the volume of the reacting solution is sufficiently small, the pH of the reacting solution decreases because the OH^- in the solution is consumed and H_2 is generated during the reaction with the Al layer.[1] Hence, a confined volume (1−10 nL) of the KOH solution loaded with poly(dimethylsiloxane) (PDMS) microstamped onto the Au nanomembrane covering the Al layer can produce protruding solid $Al(OH)_3$ features on the Au nanomembrane that can then be utilized in millimeter-scale flexible THz responsive, dielectric/metal photonic structures.[1]

In this study, scanning probe lithography (SPL) is used to load a small volume, i.e., hundreds of attoliters (aL) to tens of femtoliters (fL), of the reacting solution (KOH) for use in Au nanomembrane-based lithography.[1,2] SPL is suitable for nano- and microfabrication because it employs a nanoscaled tip to fabricate structures on a substrate. Dip-pen nanolithography (DPN) is one of SPL that directly delivers inked materials from the nanoscaled tip to the substrate, where the inked material, the tip, and the substrate operate together as an "ink-pen-paper" system.[4] Therefore, organic molecules,[5−7] nanoparticles,[8−11] proteins,[12,13] and polymers[14,15] can be directly patterned onto a substrate using DPN. Polymer-pen lithography (PPL) is a similar tool to DPN in that it directly delivers ink materials, as it employs an array of potentially millions of elastomeric pyramid-shaped pens made from PDMS to transfer ink to a large-area substrate.[16]

In principle, both liquid- and solid-phase ink materials can be used with DPN and PPL.[4,17−20] Solid-ink materials are diffusive and transferred through the water meniscus that naturally forms between the tip and the substrate surface via condensation from the ambient humidity. In contrast, liquid ink is directly transferred from the tip to the substrate surface, in which the water meniscus is not formed because the ink is liquid itself. Due to the larger volume of liquid ink loaded onto the tip probe compared to the water meniscus formed in solid-ink printing, larger patterns are typically obtained using liquid-

Received: January 3, 2023
Accepted: February 23, 2023
Published: March 8, 2023

ink printing. However, micron-scale patterns can be produced by taking advantage of the much shorter dwell time of liquid-ink printing compared with solid-ink printing. For instance, patterned lines as small as 15-nm wide have been reported for solid inks (alkanethiols),[21] while a subcellular-scale template for protein binding has been fabricated using liquid inks (liquid silanes) with a dwell time of approximately 1 s.[12] Indeed, due to the small reacting volume of the meniscus, DPN can be used to facilitate novel chemical reactions for the synthesis of materials that would otherwise not be possible on a bulk scale.[21−23]

In the present study, a small volume (100 aL to 10 fL) of the KOH solution is placed on an Au nanomembrane on an Al layer using DPN and PPL to verify that the fabrication of protruding $Al(OH)_3$ structures reported for Au nanomembrane lithography can be reproduced on a sub-microscale. KOH aqueous solution ink (1 M) is loaded onto a tip probe and DPN printing is carried out either immediately (i.e., liquid-ink printing) or after the ink solution has dried (i.e., solid-ink printing). Micron-sized ($\geq$6 μm) dots of $Al(OH)_3$ with KOH salts are obtained using liquid-ink printing, and sub-micron-sized ($\approx$800 nm) dots of $Al(OH)_3$ are obtained with solid-ink printing, with the presence of $Al(OH)_3$ confirmed using electron probe microanalysis (EPMA) and time-of-flight secondary ion mass spectrometry (ToF-SIMS). In addition, arrays of $Al(OH)_3$ features with micron ($\geq$4 μm) and sub-micron (minimum $\approx$300 nm) sizes are produced on a millimeter-sized area of the Au nanomembrane on the Al layer using PPL with liquid and solid KOH inks, respectively. Moreover, yields of the fabricated $Al(OH)_3$ features through solid- and liquid-ink printings are estimated by approximating the reacting volume of the ink solution in each printing, which is discussed with ink transfer kinetics.[24] Our demonstration clearly shows that the decrease in the pH of the reacting solution, which facilitates $Al(OH)_3$ solidification, occurs with a small volume of the reacting solution in Au nanomembrane-based lithography. Moreover, the nano/microfabrication of $Al(OH)_3$ occurs with a relatively small volume of ink in ambient conditions without the need for a previously reported molding process,[1] which suggests that Au nanomembrane-based lithography in conjunction with SPL would be useful for applications that require inorganic nano- or microstructures to be arranged in on-demand patterned designs.

EXPERIMENTAL SECTION

Materials. KOH was purchased from Sigma-Aldrich (semiconductor grade 99.99%, Korea). Al (99.999%) and Au (99.99%) sources were purchased from iTASCO in Korea. Si wafers (4 in.) purchased from Sehyoung-wafertech Co., Ltd. (Korea) were used as the substrate for Au/Al multifilm thermal deposition under a pressure of 10^{-6} Torr (KVE-T2000, Korea Vacuum Tech. Ltd., Korea). A 100 nm thick Al layer was deposited on the Si substrate, and a 20 nm thick Au layer was then deposited on the Al layer. The deposition rate for the Al and Au layers was ~0.1 Å/s.

DPN and PPL Printing. To fabricate $Al(OH)_3$ structures using DPN and PPL printing, a SiN-tipped cantilever (12 pens, M-1 type, Advanced Creative Solutions Technology (ACST) LLC) (Figure S6a) and a polymer pen with an array (1.5 cm × 1.5 cm) of 140,625 pyramidal-shaped tips (Figure S6b) were treated with O_2 plasma for 30 s, followed by sequential immersion in 2 mL of the 1 M KOH ink solution for 2 min.

For liquid-ink DPN printing, the KOH-inked SiN-tipped cantilever was immediately installed on the nanolithography platform (DPN5000, ACST LLC) and engaged to the surface of the Au/Al-layered Si substrate. The tip was placed on the surface for a dwell time of 1 s in 50% humidity in a humidity chamber. The controllability of liquid-ink DPN printings (Figure 2b) was characterized by the patterns fabricated by the same batch of the printings; the error bars shown in Figure 2b-III,IV are standard deviations of the patterns fabricated by one run of printing by the multipen. The DPN-printed samples were sequentially rinsed with deionized (DI) water and dried using a flow of N_2 gas. To produce large-area patterned $Al(OH)_3$ structures using liquid-ink PPL printing, the polymer pen was inked using the same steps as for liquid-ink DPN printing. However, an atomic force microscope (AFM) (TT-2 AFM, AFM Workshop) upgraded for lithography was used in a humidity chamber at 30% humidity for liquid-ink PPL printing. A dwell time of approximately 1 s is used for liquid-ink PPL printing.

For solid-ink printing, both the KOH-inked SiN-tipped cantilever and the polymer pen were dried for 20 min in ambient conditions. The inked SiN tip and polymer pen were installed in the DPN5000 and TT-2 AFM, respectively. For solid-ink DPN printing, the tip was left in contact with the substrate for 10 min in a humidity chamber at 50% humidity. For solid-ink PPL printing, the polymer pen was left in contact with the substrate for 30 min in a humidity chamber at 30% humidity. Because the KOH salts loaded on the tip and pen during solid-ink printing can absorb water when environmental humidity increases, the solid-ink DPN and PPL printings can change like liquid-ink printing if the humidity excessively increases. Thus, 50% humidity and 30% humidity are the maximum humidity for the solid-ink DPN and PPL printings, respectively. It is assumed that polymer pens used in PPL are more easily wet by their superior absorption capability than SiN tips used in DPN, which would result in the different maximum humidity of the solid-ink PPL printing compared to that of the solid-ink DPN printing. For both liquid- and solid-ink printing, post-processing involved the gentle rinsing of the printed samples with DI water.

Sample Characterization. *Kelvin Probe Force Microscopy (KPFM).* Topographic, phase, and surface-potential images of the DPN-printed $Al(OH)_3$ dots using liquid-ink (diameter under 6 μm; Figures S3 and S4) and solid-ink printing (Figures 3 and S3) were analyzed using an AFM in amplitude-modulated KPFM mode (Dimension Icon, Bruker Co.) with a Pt/Ir-coated tip (SCM-PIT, Bruker Co.). For the measurement of the surface potential, tip scanning in an area of interest was carried out at 0.55 Hz using a lift height of 10 nm.

Electron Probe Microanalysis (EPMA). EPMA was carried out with a field emission electron probe microanalyzer (JXA-8530F, JEOL Ltd., Japan) to characterize the elements present in the $Al(OH)_3$ dots fabricated using liquid-ink DPN printing. EPMA maps (50 μm × 50 μm; 250 × 250 pixels) of Al, O, Au, and K were obtained using an electron beam source accelerated by a voltage of 15 kV with a probe current of 60 nA.

Time-of-Flight Secondary Ion Mass Spectrometry (ToF-SIMS). Elemental characterization of the $Al(OH)_3$ dots fabricated using DPN solid-ink printing was conducted using a TOF-SIMS 5 (ION-TOF GmbH, Germany) with a pulsed 30 keV Bi^+ primary beam and a current of 0.55 pA for a data acquisition time of 500 s. The Al^+ ion spectrum was internally

https://doi.org/10.1021/acsomega.3c00038
ACS Omega 2023, 8, 10439−10448

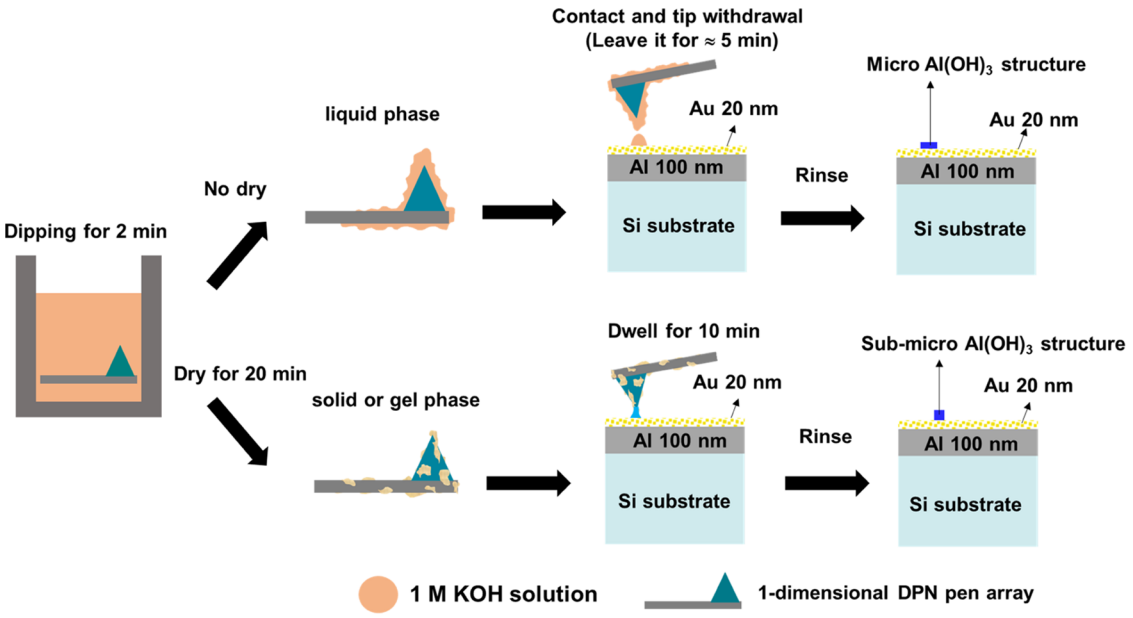

Figure 1. Schematic diagrams for $Al(OH)_3$ fabrication using (top) liquid- and (bottom) solid-ink printing via DPN with KOH ink.

calibrated using H^+, CH_3^+, $C_2H_5^+$, $C_3H_7^+$, and $C_4H_9^+$, which were normalized to the respective secondary total ion yields. A chemical image of the analyzed area (Figure 3b-II) was captured at 512 × 512 pixels. The depth profile (Figure 3b-III) was obtained by the one-time running of etching at the analyzed area (500 μm × 500 μm) with a Cs beam accelerated at 250 eV for 7600 s.

RESULTS AND DISCUSSION

Figure 1 presents schematic diagrams of the fabrication of $Al(OH)_3$ structures on the Au/Al-layered (20 nm/100 nm) Si substrate using DPN and KOH ink. The one-dimensional (1D) pen array is dipped in a 1 M KOH aqueous solution for 2 min to load the KOH ink onto the tip. For liquid-ink printing, DPN printing with the KOH ink-loaded pen array is carried out immediately without drying. A small volume of the KOH solution is delivered to the substrate surface with a relatively short dwell time (~1 s), acting as a source of OH^- that penetrates the 20 nm thick Au nanomembrane and chemically reacts with Al.[1] The volume of the KOH ink solution delivered using liquid-ink DPN printing was approximately tens of femtoliters, estimated based on the contact angle of the ink solution on the substrate (Figure 5d). The KOH solution was left undisturbed on the surface for approximately 5 min to allow sufficient time for the chemical reaction to occur. The concentration of OH^- in the reacting solution decreased, thus reducing its pH, due to the chemical reaction with the Al layer to form soluble $Al(OH)_4^-$ (Figure S2). Microscale $Al(OH)_3$ structures were obtained via $Al(OH)_3$ solidification.

For solid-ink printing, DPN printing with the KOH ink-loaded pen array was conducted after drying the ink solution for 20 min. Unlike liquid-ink printing, the ink-loaded pen array had a relatively long dwell time (10 min), allowing a meniscus to form between the tip of the pen array and the substrate that dissolved the dried KOH salts, producing a reacting solution that acted as a source of OH^-. For DPN solid-ink printing, the volume of the reacting solution was estimated to be hundreds of attoliters (Figure 5d). As a result, sub-micron $Al(OH)_3$ structures were obtained following $Al(OH)_3$ solidification.

Figure 2 shows the details of liquid-ink DPN printing. Figure 2a-I presents a schematic diagram of the liquid-ink printing process using DPN with KOH ink. $Al(OH)_3$ microstructures were fabricated on the Au/Al-layered Si substrate following the application of the KOH solution in conjunction with sufficient time for $Al(OH)_3$ solidification to occur, followed by rinsing with DI water. Figure 2a-II shows optical microscopy (OM) images of the dot pattern fabricated using liquid-phase 1 M KOH ink DPN printing with a dwell time of 1 s; the left and right images are of the dot pattern before and after rinsing with DI water, respectively. The residue on the dot pattern was removed by DI, indicating that KOH salts were formed using this liquid-ink printing process. It is assumed that the KOH salts on the dot pattern formed as the water solvent in the reacting solution dried during the $Al(OH)_3$ solidification process. The removal of the KOH salts was confirmed with the dark-mode OM image presented in Figure 2a-III following exposure of the dot pattern shown in the right-side image of Figure 2a-II to H_2O vapor. Bubbles generated following H_2O vapor exposure were only absent in the area holding the dot pattern, which would be hydrophilic if KOH salts were present.

As shown in Figure 2b-I, the dimensions of the dot pattern shown in the right-side image in Figure 2a-II were measured with tapping-mode AFM, while the cross-sectional line profile for the white line in Figure 2b-I is displayed in Figure 2b-II. The diameter (D) and height (h) of the dot pattern were 12.1 ± 0.2 μm and 35.9 ± 6.2 nm, respectively. The diameter of the dot pattern in liquid-ink DPN printing can be controlled by reducing the volume of the ink loaded onto the tip probe using repeated cycles of brief contact with the substrate.[12] Figure 2b-III presents the relationship between the number of times the KOH-ink-loaded tip was placed in contact with the Au/Al substrate and the diameter of the resulting dot pattern. When the tip was placed in contact with the substrate the first time, the size of the dot was 12.1 ± 0.2 μm; this decreased to 6.8 ± 0.2 μm the 10th time the tip came into contact with the substrate. This decreasing diameter of the dot pattern depending on the increasing number of contacts would result from a typical ink depletion reported in liquid ink transport of

https://doi.org/10.1021/acsomega.3c00038
ACS Omega 2023, 8, 10439−10448

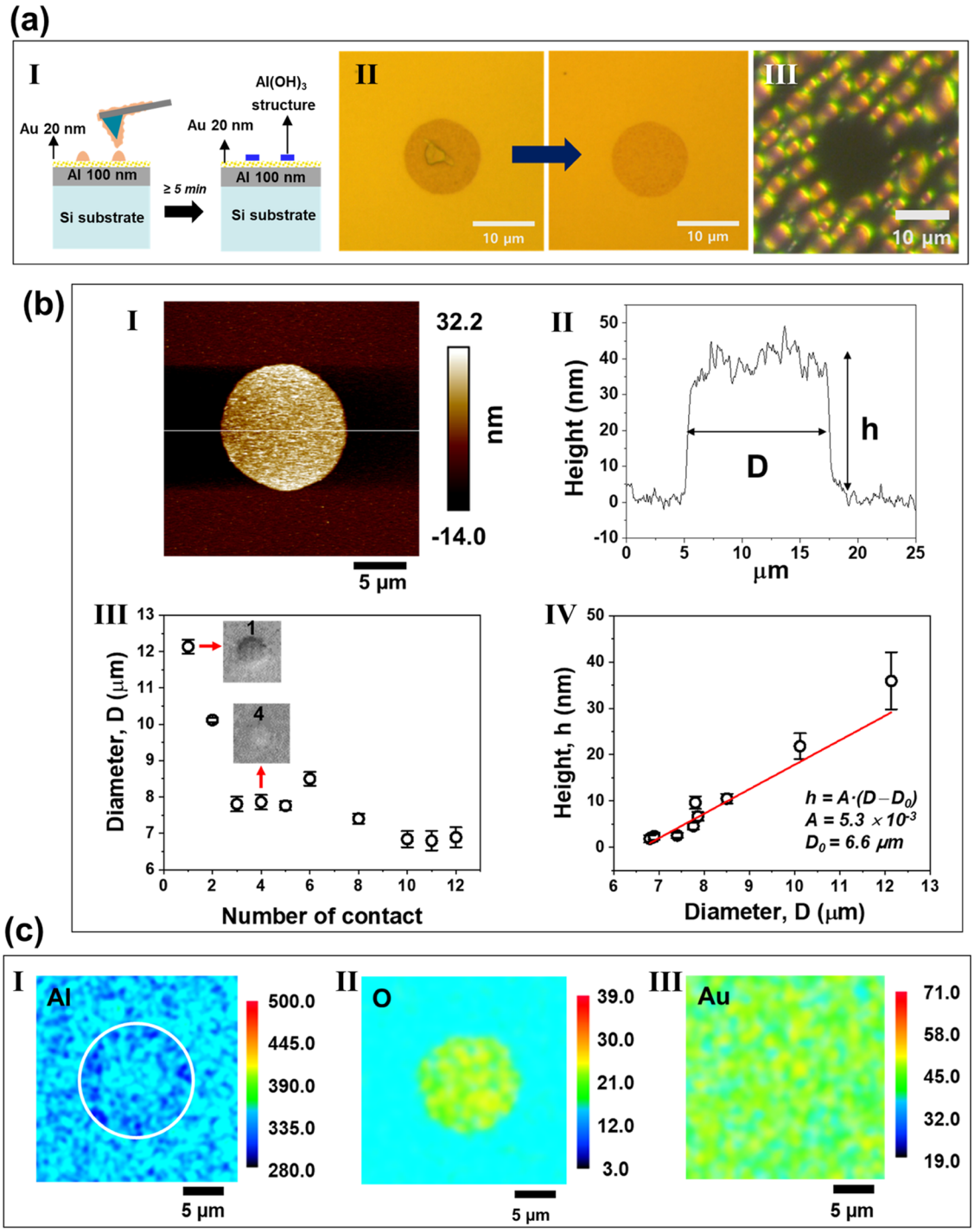

Figure 2. Liquid-ink DPN printing. (a) Printing process: (I) schematic diagram of liquid-ink printing with DPN using KOH ink; (II) optical microscopy (OM) images of an $Al(OH)_3$ dot fabricated using liquid-ink DPN printing: (left) before and (right) after rinsing with DI water; and (III) dark-mode OM image of the right-side image in panel (II) after exposure to H_2O vapor. (b) Controllability of printing: (I) topographic tapping-mode AFM image of the right-side image of panel (II) in panel (a); (II) cross-sectional line profile of the $Al(OH)_3$ dot taken along the white line in panel (I). D and h represent the diameter and height of the $Al(OH)_3$ dot, respectively; (III) relationship between the number of times contact is made between the tip and the surface and the diameter of the $Al(OH)_3$ dots. Inset: scanning electron microscopy (SEM) images of the $Al(OH)_3$ dots after the first contact (1) and the fourth contact (4), respectively; and (IV) height of the $Al(OH)_3$ dots in relation to their diameter. The linearly fitted line is marked in red; its slope is 5.3×10^{-3}. (c) Elemental characterization: EPMA maps of the $Al(OH)_3$ dot for (I) Al, (II) O, and (III) Au. The white line in (I) represents the dot pattern.

DPN printings.[25,26] In addition, the height (h) of the dot increased linearly with the diameter (D), with a minimum diameter of 6.6 μm (Figure 2b-IV). The linear relationship between the pattern height and diameter has been previously reported for physisorption-based ink in DPN printing; for example, the height of poly(ethylene glycol) (PEG) dots printed using DPN has a linear dependence on diameter, with an aspect ratio (h/D) of 0.1−0.3.[27] Figure 2b-IV shows that

https://doi.org/10.1021/acsomega.3c00038
ACS Omega 2023, 8, 10439−10448

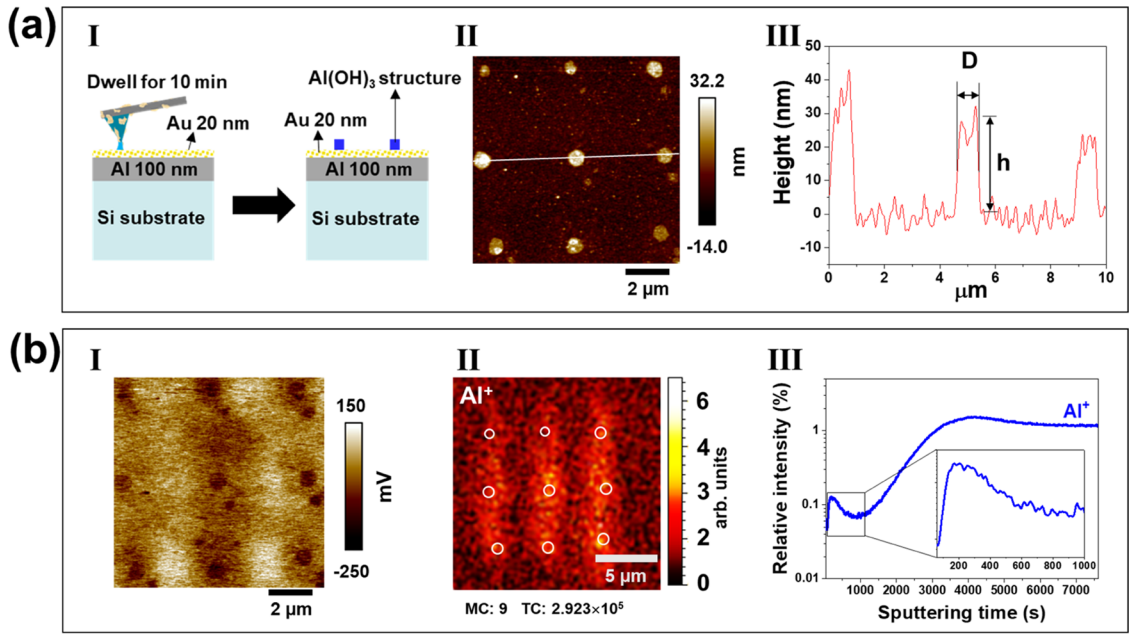

Figure 3. Solid-ink DPN printing. (a) Printing process and patterns: (I) schematic diagram of solid-ink printing with DPN using KOH ink; (II) topographic AFM image of the $Al(OH)_3$ dot array fabricated using solid-ink DPN printing; and (III) cross-sectional line profile of the $Al(OH)_3$ dot array taken along the white line in panel (II). *D* and *h* represent the diameter and height of the $Al(OH)_3$ dots, respectively. (b) Elemental characterization: (I) surface-potential image of panel (II) in panel (a) taken using KPFM; (II) intensity map for Al^+ ions in the $Al(OH)_3$ dot array measured using ToF-SIMS (the white circles denote the $Al(OH)_3$ dots). MC: maximal counts in one pixel and TC: total counts in the image; and (III) depth profile for the Al^+ ions obtained from panel (II).

the aspect ratio of the dot pattern, i.e., the slope of the linearly fitted line, was 5.3×10^{-3}. The smaller aspect ratio of the dot patterns in the present study compared to the previously reported PEG patterns indicates that pattern fabrication using $Al(OH)_3$ solidification has a lower yield than physisorption-based DPN printing. The lower yield of $Al(OH)_3$ solidification may result from the water solvent in the reacting solution drying during the $Al(OH)_3$ solidification process, which can result in the formation of the KOH salts, preventing all of the OH^- ions in the reacting solution from participating in the $Al(OH)_3$ solidification process.

The chemical elements present in the dot patterns fabricated using liquid-ink printing via DPN with KOH ink were characterized using EPMA (Figure 2c). Figure 2c-I presents an EPMA map for Al, with the white line representing the dot pattern. A lower EPMA intensity for Al was observed within the dot pattern than outside it. It has been reported that the EPMA intensity of a metal element within an oxidized area is lower than that in a nonoxidized region due to the greater volume of the metal oxide.[28] It was also found that the intensity for O was much higher in the dot pattern than outside it (Figure 2c-II), indicating that the dot pattern is composed of an oxidized aluminum component such as $Al(OH)_3$. Figure 2c-III shows that there was a uniform EPMA intensity for Au, indicating that the Au nanomembrane was not damaged during the $Al(OH)_3$ solidification process described in Figure 2a-I.

The results for solid-ink printing using DPN with KOH ink are summarized in Figure 3. After drying the KOH ink solution, the DPN pen was placed on the Au/Al-layered Si substrate with a longer dwell time than that used for liquid-ink printing, leading to the fabrication of sub-micron $Al(OH)_3$ structures via $Al(OH)_3$ solidification in the meniscus that formed between the tip and the substrate (Figure 3a-I). Figure 3a-II shows an AFM topographical image of a 3×3 $Al(OH)_3$ dot array fabricated using solid-ink printing with DPN and a dwell time of 10 min. The DPN printing began with the dot in the top-left corner and then continued from left to right and from top to bottom. The relatively smaller dots in the top-left and top-middle positions suggest that the solid-phase KOH ink printing had not yet fully stabilized and that there had been an insufficient dissolution of KOH into the meniscus. In addition, the dots are not arranged perfectly; it can be assumed that the formation of the meniscus was affected by changes in the morphology of the tip caused by the inhomogeneous coverage of KOH ink on the tip surface that reduced as the printing process continued. This variation in the menisci during the DPN printing process would thus have influenced the positions of the $Al(OH)_3$ dots. The height and diameter of the dots were measured for the cross-sectional line shown in Figure 3a-II, with the results presented in Figure 3a-III. The height of the dots had a range of 26.9−42.7 nm, with a diameter (full width at half maximum of the peaks in Figure 3a-III) of approximately 800 nm.

The surface potential of the sample shown in Figure 3a-II was measured using KPFM (Figure 3b-I). The dots exhibited a lower surface potential than did the Au film, indicating that they were not composed of the same Au material. To confirm the fabrication of the dot array via $Al(OH)_3$ solidification, an intensity map for Al^+, which should be abundant in $Al(OH)_3$, for the 3×3 dot array was obtained using TOF-SIMS measurements (Figure 3b-II). The intensity of Al^+ near the 3×3 dots (the white circles in Figure 3b-II) was higher than in the other areas. In addition, a depth profile for Al^+ in the area of the 3×3 dot array is displayed in Figure 3b-III. The immediate rise in Al^+ intensity until ∼200 s and the gradual decline thereafter indicates that $Al(OH)_3$ structures were present on the sample surface. Because the Au film was ion-

https://doi.org/10.1021/acsomega.3c00038
ACS Omega 2023, 8, 10439−10448

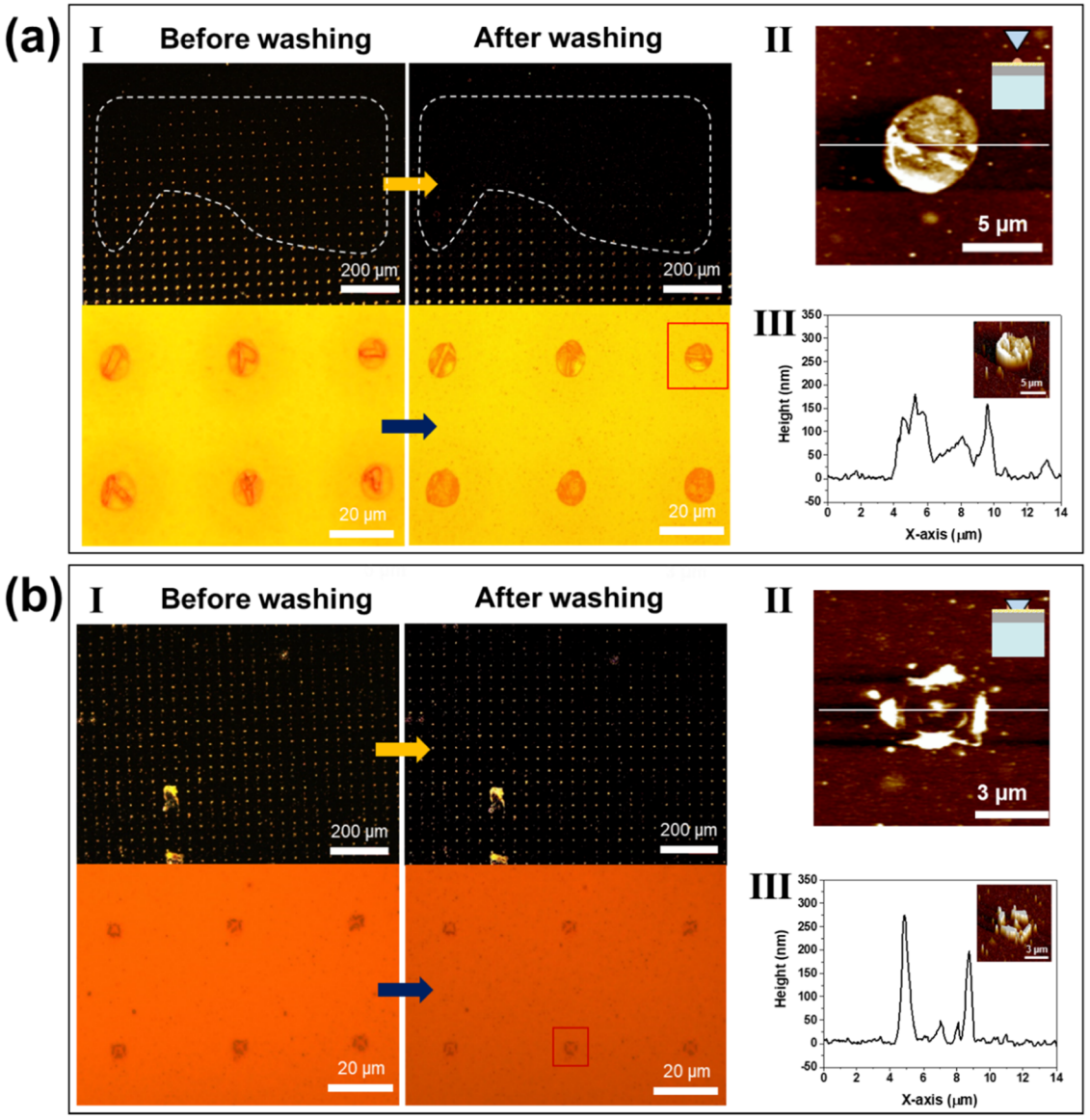

Figure 4. Liquid- and solid-ink PPL printing. (a) Liquid-ink PPL printing: (I) OM images of the patterns fabricated using liquid-ink PPL printing before and after washing with DI taken in (top) dark and (bottom) bright modes. The region where the pattern disappears following washing with DI is marked by the white dashed line; (II) topographic AFM image of the dot fabricated using liquid-ink PPL printing marked by the red box in panel (I). Inset: schematic diagram of the printing process; and (III) cross-sectional line profile taken along the white line in panel (II). Inset: the three-dimensional (3D) image of panel (II). (b) Solid-ink PPL printing: (I) OM images of the patterns fabricated using solid-ink PPL printing before and after washing with DI taken in (top) dark and (bottom) bright modes; (II) topographic AFM image of the nanostructures fabricated using solid-ink PPL printing marked by the red box in panel (I). Inset: schematic diagram of the printing process; and (III) cross-sectional line profile taken along the white line in panel (II). Inset: the 3D image of panel (II).

etched away and the underlying Al layer was exposed, the Al^+ intensity grew again from ∼1000 s and remained nearly constant after ∼3500 s.

The results for liquid- and solid-ink printing using PPL with KOH ink are summarized in Figure 4. The top OM images in Figure 4a-I, which were taken in the dark-field mode, show the patterns fabricated with liquid-ink printing via PPL before and after gentle DI washing. The array of $Al(OH)_3$ patterns was generated over a millimeter-sized area. Figure 4a-I shows that the size of dot patterns at the top looks smaller than that of dot patterns at the bottom, which would be caused by imperfect leveling between the polymer-pen array and the substrate during the PPL printing.[29] In addition, zoomed OM images taken in the bright-field mode of the patterns are presented at the bottom of Figure 4a-I, showing that the KOH salt residue on the patterns was removed by DI, as with the liquid-ink printing using DPN (Figure 2a-II). The smaller patterns inside the dashed line disappeared after washing with DI, which was consistent with the observation in Figure 2b-IV that $Al(OH)_3$ patterns smaller than ∼6.6 μm were difficult to obtain using liquid-ink printing. This means that KOH salts were more readily formed in the smaller reacting solution during the liquid-ink printing process due to the faster removal of water from the reacting solution.

Figure 4a-II presents a topographic AFM image of the dot marked by the red box in Figure 4a-I fabricated using liquid-ink PPL printing. In Figure 4a-III, the cross-sectional line profile obtained from the white line present in Figure 4a-II

https://doi.org/10.1021/acsomega.3c00038
ACS Omega 2023, 8, 10439−10448

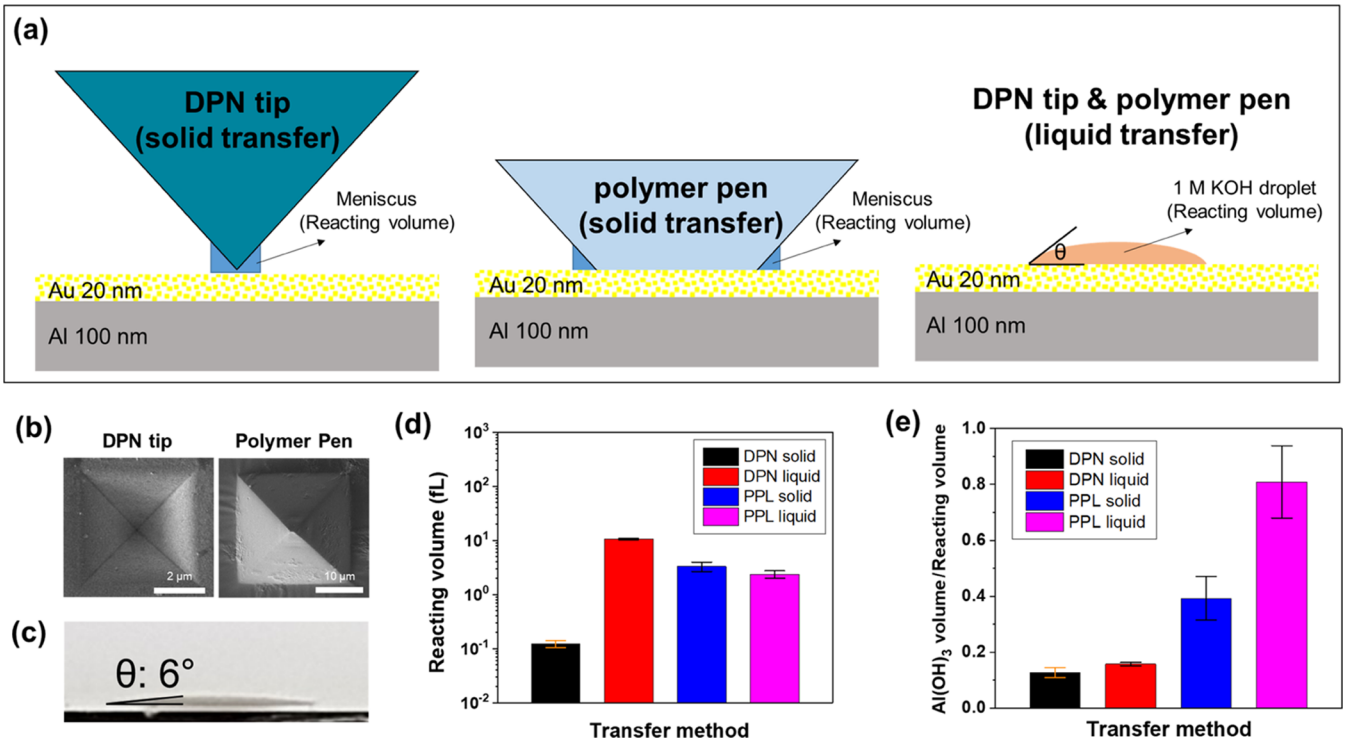

Figure 5. (a) Schematic diagrams of the reacting volumes for $Al(OH)_3$ solidification in liquid- and solid-ink printing using DPN and PPL. (b) SEM images of the DPN tip and the end of the polymer pen. (c) Side-view OM image of a 1 M KOH droplet on the Au/Al-layered Si substrate. (d) Reacting volume for liquid- and solid-ink printing using DPN and PPL. (e) Ratio of the protruding $Al(OH)_3$ volume to the reaction volume in liquid- and solid-ink printing with DPN and PPL.

shows that the diameter of the dot was about 6 μm; however, the minimum diameter of the dots fabricated using this printing method was approximately 4 μm (Figures S7 and S8). The removal of the KOH salts was confirmed by the recessed line profile shown in Figure 4a-III and the accompanying three-dimensional (3D) AFM image (the inset of Figure 4a-III).

OM images taken in both dark and bright modes of the patterns fabricated using solid-ink printing with PPL before and after DI washing are displayed in Figure 4b-I. More uniform patterns were generated using this printing method than with liquid-ink PPL printing, with little change observed in the patterns before and after DI washing. Interestingly, in the image in Figure 4b-II, which was taken of the area marked by the red box in Figure 4b-I, nanostructures that appear to have been produced from the meniscus that formed on the sides of the pyramidal polymer pen were observed instead of dots. The cross-sectional line profile of these nanostructures obtained from the white line in Figure 4b-II as shown in Figure 4b-III and a 3D AFM image (the inset of Figure 4b-III) indicates that sub-micron $Al(OH)_3$ structures (minimum ≈300 nm) were generated using solid-ink PPL printing over an area of more than a square millimeter (Figure 4b-I).

Figure 5 presents the results for the characterization of the reacting volume and fabrication yield for $Al(OH)_3$ fabrication on a sub-microscale using liquid and solid KOH ink printing with DPN and PPL. Figure 5a presents schematic diagrams showing the reacting volumes for $Al(OH)_3$ solidification using liquid and solid-ink printing with DPN and PPL. In solid-ink DPN printing, the reacting volume is considered to be the volume of the meniscus that forms around the end of the DPN tip; the meniscus always exists when the tip contacts the surface of the substrate in the case of solid-ink printing.[30] The distance from the end of the DPN tip to the surface of the substrate is assumed as 40 nm (the maximum height of the $Al(OH)_3$ dot pattern shown in Figure 3a-III). The surface area of the meniscus in contact with the surface can be determined using the area of the $Al(OH)_3$ dot pattern measured with AFM (Figure 3a-II) if it presumes that $Al(OH)_3$ is fully solidified in the area of the meniscus forming around the end of the DPN tip. Also, it is estimated that the meniscus would be formed as a cylindrical shape surrounding the DPN tip due to the surface tension. Then, the reacting volume of the meniscus can be obtained by subtracting the volume of the DPN tip (considered as a pyramid, as shown in Figure 5b) from that of the cylinder that has the area of the $Al(OH)_3$ dot pattern and the height of determining as the length of the line vertically drawn from the edge of the area of the $Al(OH)_3$ dot pattern to the meet point with the DPN tip, as described in the left diagram of Figure 5a. The reacting volume of the meniscus was found to be approximately 120 aL in the present study (Figure 5d).

In solid-ink PPL printing, the end of the polymer pen is deformed during printing.[16,18,31] Also, the shape of the meniscus that forms around the polymer pen when it touches the substrate is assumed as a cube-like shape based on the fabricated $Al(OH)_3$ nanostructure through solid-ink PPL printing (Figure 4b-II). The different shape of the meniscus of the solid-ink PPL printing compared to that of the solid-ink DPN printing would be supposed to result from the deformation of the polymer pen during printing. As a result, the reacting volume is regarded as the volume of the meniscus that forms around the polymer pen when it touches the substrate, as shown in the middle diagram of Figure 5a. The

https://doi.org/10.1021/acsomega.3c00038
ACS Omega 2023, 8, 10439−10448

volume of the meniscus can be calculated by subtracting the volume of the end of the pen (approximated as a truncated pyramid; Figure 5b) from a cube whose size is determined based on the $Al(OH)_3$ nanostructure, as shown in Figure 4b-II. Using this method, the reacting volume for solid-ink PPL printing was calculated to be approximately 3.3 fL.

The reacting volume for liquid-ink printing with DPN and PPL is considered to be the volume of the KOH ink droplet on the sample surface (the right-side diagram in Figure 5a), which is formed on the surface by rupturing the capillary bridge of the fluidic ink in case of liquid-ink printings (Figure S1).[32] The volume of this droplet can be calculated using assumptions that the contact area of the droplet is equal to the area of the $Al(OH)_3$ dot patterns (Figures 2b-I and 4a-II) and the contact angle of the KOH ink droplet on the sample surface is invariant depending on its volume. Thus, the contact angle (6°) between the KOH 1 M solution and the Au/Al-layered Si substrate is empirically measured, as shown in Figure 5c. As a result, the reacting volume for liquid-ink printing with DPN and PPL was assumed to be 10.6 and 2.4 fL, respectively (Figure 5d). The error bars in Figure 5d were determined from standard deviations of the $Al(OH)_3$ structures that were used for the calculation of reacting volumes.

Figure 5e displays the yield of the protruding $Al(OH)_3$ structures for liquid- and solid-ink printing using DPN and PPL, supposedly calculated as the ratio of the volume of the patterned $Al(OH)_3$ to the reacting volume shown in Figure 5d. The error bars in Figure 5e were propagated from that of the reacting volume and standard deviations of the volume of the fabricated $Al(OH)_3$ structures. Figure 5e shows that the yield for liquid-ink printing was higher than that for solid-phase printing due to the greater number of OH^- ions in the reacting solution for liquid-ink printing. The reacting solution for liquid-ink printing is directly transferred to the sample surface from the DPN tip and the polymer pen, while the OH^- ions in the reacting solution for solid-phase printing derive from the dried KOH salts on the DPN tip and the polymer pen that are dissolved in the meniscus.

PPL printing also had a higher yield than DPN printing (Figure 5e), which might be influenced by the tip intervals and the size of the printing arrays. The distance between the pens in the two-dimensional (2D) polymer-pen array was 40 μm, compared to 100 μm for the 1D DPN pen array, while the size of the 2D polymer-pen array (1.5 cm × 1.5 cm) was much larger than that of the 1D DPN pen array (1 mm). Because the underlying Al layer had a larger reacting area than the area of the protruding $Al(OH)_3$ pattern (Figure S2), the closer tip intervals may have influenced the efficiency of $Al(OH)_3$ solidification.

Also, the different yields between PPL and DPN printings would be understood by considering the transfer kinetics of the printing.[24] It was reported that the transport rate of DPN ink materials to the substrate proportionally increases as the surface area of the ink on the DPN tip increases.[24] The surface area of the ink on the tip can be controlled by adding up the number of ink material loading on the tip.[24] In short, the surface area of the ink is a dominant factor in determining the transport rate in the case of alkanethiol-ink patterning by DPN printing. On the contrary, according to our group's previous report, the higher yield of $Al(OH)_3$ structures is observed in the relatively smaller volume of the reacting solution,[1] which can be explained by the fact that $Al(OH)_3$ solidification is favorable with effective pH decrease in a sufficiently small volume of the reacting solution. Interestingly, Figure 5d,e shows that the overall yield of $Al(OH)_3$ structures does not proportionally increase depending on the reacting volume. This result would reflect that another factor besides the pH-dependent solidification is involved in the fabrication of the $Al(OH)_3$ structures. It assumes that a factor like the surface area of the ink on the tip in the alkanethiol-ink DPN printing would take part in the solidification of $Al(OH)_3$ during the KOH ink DPN and PPL printings. This assumption can give a clue why the yield of the PPL printings is higher than that of DPN printings. Due to the property of PDMS materials, polymer pens can absorb more inks compared to DPN tips, which would work similarly as a broader surface area of the ink to result in a faster transfer rate of the alkanethiol ink during the DPN printings.

Although the nano/microfabrication of $Al(OH)_3$ is demonstrated by the DPN and PPL printings with the small volume (100 aL to 10 fL) of the KOH solution in ambient conditions without requiring a previously reported molding process,[1] the demonstrated method requires the condition that the meniscus, acting as the reaction site during $Al(OH)_3$ solidification, needs to be stationary and stable. This required condition of the meniscus for $Al(OH)_3$ solidification is inferred by the facts that the around 10 min of dwell time to fabricate a single nano/microstructure of $Al(OH)_3$ dots and the unavailable fabrication of line patterns of $Al(OH)_3$ (Figure S5). In the case of the line patterning, the tip moves with scan speeds of 0.005−0.5 μm/s, where the meniscus is not stationary and stable during the patterning. However, the use of multipen and stipple patterns can help to improve the throughput and the design capability of the demonstrated $Al(OH)_3$ fabrication method. In addition, other liquid ink printing methods (i.e., ink-jet, electrohydrodynamic printer, and micropipette) would also be used for nano/microfabrication of $Al(OH)_3$ if the relatively small volume of the KOH solution can be equipped with.

CONCLUSIONS

Employing Au nanomembrane-based lithography, this study demonstrated that DPN and PPL facilitate the chemical reaction of a small volume of the KOH ink solution (100 aL to 10 fL) on an Au/Al (20/100 nm)-layered Si substrate, leading to the fabrication of protruding $Al(OH)_3$ structures in ambient conditions. Because liquid-ink printing with DPN and PPL directly transfers KOH droplets to the substrate surface, it is more advantageous than solid-ink printing in terms of processing time and yields for $Al(OH)_3$ fabrication. However, sub-micron-sized $Al(OH)_3$ structures can be obtained using solid-ink printing with DPN and PPL because the meniscus formed between the pen and the substrate limits the dimensions of the reacting solution for $Al(OH)_3$ solidification. Therefore, liquid- or solid-ink printing can be selected depending on the purpose of $Al(OH)_3$ fabrication, particularly whether the processing time or the resolution is the main priority. The success of the $Al(OH)_3$ fabrication method proposed in this paper, with its relatively small reacting solution volume and ability to be conducted in ambient conditions, suggests that Au nanomembrane-based lithography in conjunction with SPL has great promise for use in various applications associated with the fabrication of localized metal oxides.

https://doi.org/10.1021/acsomega.3c00038
ACS Omega 2023, 8, 10439−10448

■ ASSOCIATED CONTENT

Supporting Information

The Supporting Information is available free of charge at https://pubs.acs.org/doi/10.1021/acsomega.3c00038.

Details of the $Al(OH)_3$ solidification process in liquid-ink printing; characterization of patterns less than 6 μm in diameter; line patterning using liquid- and solid-ink DPN printing; images of the DPN tip array and the polymer pen; dot patterns fabricated using liquid-ink PPL printing; and summary table of the different printing modes (PDF)

■ AUTHOR INFORMATION

Corresponding Authors

Dong Hyuk Park − *Department of Chemical Engineering, Program in Biomedical Science & Engineering, Inha University, Incheon 22212, Republic of Korea*; Email: donghyuk@inha.ac.kr

Jae-Won Jang − *Division of Physics and Semiconductor Science, Dongguk University, Seoul 04620, Republic of Korea; Quantum-Functional Semiconductor Research Center, Dongguk University, Seoul 04620, Republic of Korea*; orcid.org/0000-0002-2162-4520; Email: jwjang@dongguk.edu, jwjang@dgu.ac.kr

Authors

Jehyeok Ryu − *Department of Physics, Pukyong National University, Busan 48513, Republic of Korea*; Present Address: Donostia International Physics Center (DIPC), Paseo Manuel de Lardizabal 4, 20018 Donostia-San Sebastián, Spain; orcid.org/0000-0002-9196-4299

Jeong-Sik Jo − *Division of Physics and Semiconductor Science, Dongguk University, Seoul 04620, Republic of Korea*; orcid.org/0000-0001-5005-3395

Jin-Hyun Choi − *Department of Physics, Pukyong National University, Busan 48513, Republic of Korea*; Present Address: Department of Physics, Ulsan National Institute of Science and Technology, Ulsan 44919, Republic of Korea.

Deuk Young Kim − *Division of Physics and Semiconductor Science, Dongguk University, Seoul 04620, Republic of Korea; Quantum-Functional Semiconductor Research Center, Dongguk University, Seoul 04620, Republic of Korea*

Jiyoun Kim − *Department of Chemical Engineering, Program in Biomedical Science & Engineering, Inha University, Incheon 22212, Republic of Korea*

Complete contact information is available at: https://pubs.acs.org/10.1021/acsomega.3c00038

Author Contributions

J.-W.J. and D.H.P. conceived the project. J.R., J.-S.J., J.-H.C., and D.H.P. performed the experiments. J.-W.J. and J.R. analyzed data and wrote the manuscript. J.-W.J., J.R., J.-S.J., J.-H.C., J.K., D.Y.K., and D.H.P. discussed and contributed to writing the manuscript.

Notes

The authors declare no competing financial interest.

■ ACKNOWLEDGMENTS

This work was supported by the National Research Foundation of Korea (NRF) grant funded by the Korea Government Ministry of Science and ICT (MSIT) (NRF-2016R1A6A1A03012877; 2021R1A4A5031805; 2022R1H1A2091399; 2022K2A9A1A01098183). Also, this work was supported by the Dongguk University Research Fund of 2020.

■ REFERENCES

(1) Oh, C.-M.; Park, K. H.; Choi, J.-H.; Hwang, S.; Noh, H.; Yu, Y. M.; Jang, J.-W. Polycrystalline Au Nanomembrane as a Tool for Two-Tone Micro/Nanolithography. *Chem. Mater.* **2017**, *29*, 3863−3872.

(2) Choi, J.-H.; Oh, C.-M.; Jang, J.-W. Micro- and nano-patterns fabricated by embossed microscale stamp with trenched edges. *RSC Adv.* **2017**, *7*, 32058−32064.

(3) Floro, J. A.; Hearne, S. J.; Hunter, J. A.; Kotula, P.; Chason, E.; Seel, S. C.; Thompson, C. V. The dynamic competition between stress generation and relaxation mechanisms during coalescence of Volmer−Weber thin films. *J. Appl. Phys.* **2001**, *89*, 4886−4897.

(4) Urtizberea, A.; Hirtz, M.; Fuchs, H. Ink transport modelling in Dip-Pen Nanolithography and Polymer Pen Lithography. *Nanofabrication* **2015**, *2*, 43−53.

(5) Hong, S.; Mirkin, C. A. A Nanoplotter with Both Parallel and Serial Writing Capabilities. *Science* **2000**, *288*, 1808.

(6) Hong, S.; Zhu, J.; Mirkin, C. A. Multiple Ink Nanolithography: Toward a Multiple-Pen Nano-Plotter. *Science* **1999**, *286*, 523.

(7) Jung, H.; Kulkarni, R.; Collier, C. P. Dip-Pen Nanolithography of Reactive Alkoxysilanes on Glass. *J. Am. Chem. Soc.* **2003**, *125*, 12096−12097.

(8) Ben Ali, M.; Ondarçuhu, T.; Brust, M.; Joachim, C. Atomic Force Microscope Tip Nanoprinting of Gold Nanoclusters. *Langmuir* **2002**, *18*, 872−876.

(9) Garno, J. C.; Yang, Y.; Amro, N. A.; Cruchon-Dupeyrat, S.; Chen, S.; Liu, G.-Y. Precise Positioning of Nanoparticles on Surfaces Using Scanning Probe Lithography. *Nano Lett.* **2003**, *3*, 389−395.

(10) Huang, L.; Braunschweig, A. B.; Shim, W.; Qin, L.; Lim, J. K.; Hurst, S. J.; Huo, F.; Xue, C.; Jang, J.-W.; Mirkin, C. A. Matrix-Assisted Dip-Pen Nanolithography and Polymer Pen Lithography. *Small* **2009**, *6*, 1077−1081.

(11) Senesi, A. J.; Rozkiewicz, D. I.; Reinhoudt, D. N.; Mirkin, C. A. Agarose-Assisted Dip-Pen Nanolithography of Oligonucleotides and Proteins. *ACS Nano* **2009**, *3*, 2394−2402.

(12) Jang, J.-W.; Collins, J. M.; Nettikadan, S. User-Friendly Universal and Durable Subcellular-Scaled Template for Protein Binding: Application to Single-Cell Patterning. *Adv. Funct. Mater.* **2013**, *23*, 5840−5845.

(13) Jonkheijm, P.; Weinrich, D.; Schröder, H.; Niemeyer, C. M.; Waldmann, H. Chemical Strategies for Generating Protein Biochips. *Angew. Chem., Int. Ed.* **2008**, *47*, 9618−9647.

(14) Maynor, B. W.; Filocamo, S. F.; Grinstaff, M. W.; Liu, J. Direct-Writing of Polymer Nanostructures: Poly(thiophene) Nanowires on Semiconducting and Insulating Surfaces. *J. Am. Chem. Soc.* **2002**, *124*, 522−523.

(15) Lim, J. H.; Mirkin, C. A. Electrostatically Driven Dip-Pen Nanolithography of Conducting Polymers. *Adv. Mater.* **2002**, *14*, 1474−1477.

(16) Huo, F.; Zheng, Z.; Zheng, G.; Giam, L. R.; Zhang, H.; Mirkin, C. A. Polymer Pen Lithography. *Science* **2008**, *321*, 1658.

(17) Brinkmann, F.; Hirtz, M.; Greiner, A. M.; Weschenfelder, M.; Waterkotte, B.; Bastmeyer, M.; Fuchs, H. Interdigitated Multicolored Bioink Micropatterns by Multiplexed Polymer Pen Lithography. *Small* **2013**, *9*, 3266−3275.

(18) Biswas, S.; Brinkmann, F.; Hirtz, M.; Fuchs, H. Patterning of Quantum Dots by Dip-Pen and Polymer Pen Nanolithography. *Nanofabrication* **2015**, *2*, 19−26.

(19) Liu, G.; Petrosko, S. H.; Zheng, Z.; Mirkin, C. A. Evolution of Dip-Pen Nanolithography (DPN): From Molecular Patterning to Materials Discovery. *Chem. Rev.* **2020**, *120*, 6009−6047.

(20) Braunschweig, A. B.; Senesi, A. J.; Mirkin, C. A. Redox-Activating Dip-Pen Nanolithography (RA-DPN). *J. Am. Chem. Soc.* **2009**, *131*, 922−923.

(21) Piner, R. D.; Zhu, J.; Xu, F.; Hong, S.; Mirkin, C. A. "Dip-Pen"; Nanolithography. *Science* **1999**, *283*, 661.
(22) Chen, P.-C.; Liu, M.; Du, J. S.; Meckes, B.; Wang, S.; Lin, H.; Dravid, V. P.; Wolverton, C.; Mirkin, C. A. Interface and heterostructure design in polyelemental nanoparticles. *Science* **2019**, *363*, 959.
(23) Ding, L.; Li, Y.; Chu, H.; Li, X.; Liu, J. Creation of Cadmium Sulfide Nanostructures Using AFM Dip-Pen Nanolithography. *J. Phys. Chem. B* **2005**, *109*, 22337−22340.
(24) Giam, L. R.; Wang, Y.; Mirkin, C. A. Nanoscale Molecular Transport: The Case of Dip-Pen Nanolithography. *J. Phys. Chem. A* **2009**, *113*, 3779−3782.
(25) Förste, A.; Pfirrmann, M.; Sachs, J.; Gröger, R.; Walheim, S.; Brinkmann, F.; Hirtz, M.; Fuchs, H.; Schimmel, T. Ultra-large scale AFM of lipid droplet arrays: investigating the ink transfer volume in dip pen nanolithography. *Nanotechnology* **2015**, *26*, No. 175303.
(26) Dawood, F.; Wang, J.; Schulze, P. A.; Sheehan, C. J.; Buck, M. R.; Dennis, A. M.; Majumder, S.; Krishnamurthy, S.; Ticknor, M.; Staude, I.; Brener, I.; Goodwin, P. M.; Amro, N. A.; Hollingsworth, J. A. The Role of Liquid Ink Transport in the Direct Placement of Quantum Dot Emitters onto Sub-Micrometer Antennas by Dip-Pen Nanolithography. *Small* **2018**, *14*, No. 1801503.
(27) Jang, J.-W.; Zheng, Z.; Lee, O.-S.; Shim, W.; Zheng, G.; Schatz, G. C.; Mirkin, C. A. Arrays of Nanoscale Lenses for Subwavelength Optical Lithography. *Nano Lett.* **2010**, *10*, 4399−4404.
(28) Dadé, M.; Esin, V. A.; Nazé, L.; Sallot, P. Short- and long-term oxidation behaviour of an advanced Ti_2AlNb alloy. *Corros. Sci.* **2019**, *148*, 379−387.
(29) Giam, L. R.; Massich, M. D.; Hao, L.; Wong, L. S.; Mader, C. C.; Mirkin, C. A. Scanning probe-enabled nanocombinatorics define the relationship between fibronectin feature size and stem cell fate. *Proc. Natl. Acad. Sci. U.S.A.* **2012**, *109*, 4377−4382.
(30) Weeks, B. L.; DeYoreo, J. J. Dynamic meniscus growth at a scanning probe tip in contact with a gold substrate. *J. Phys. Chem. B* **2006**, *110*, 10231−10233.
(31) Liao, X.; Braunschweig, A. B.; Zheng, Z.; Mirkin, C. A. Force- and Time-Dependent Feature Size and Shape Control in Molecular Printing via Polymer-Pen Lithography. *Small* **2009**, *6*, 1082−1086.
(32) Eichelsdoerfer, D. J.; Brown, K. A.; Mirkin, C. A. Capillary bridge rupture in dip-pen nanolithography. *Soft Matter* **2014**, *10*, 5603−5608.

https://doi.org/10.1021/acsomega.3c00038
ACS Omega 2023, 8, 10439−10448